Hindawi
Mathematical Problems in Engineering
Volume 2020, Article ID 3804748, 15 pages
https://doi.org/10.1155/2020/3804748

Research Article

Hydrodynamic Analysis of Ship with Well Deck in the Linear Numerical Wave Tank

Gang Xu,[1] **Tian-Rui Mei**,[1] **Ming-Liang Hu**,[2] **Zhen Chen**,[1] **and Jun-Ming Hu**[1]

[1]*Marine Equipment and Technology Institute, School of Naval Architecture and Ocean Engineering, Jiangsu University of Science and Technology, Zhenjiang 212003, China*
[2]*Boat R&D Center, Hubei Sanjiang Boats Science & Technology Co. Ltd, Xiaogan 432000, China*

Correspondence should be addressed to Jun-Ming Hu; Junming5779@126.com

Received 16 October 2019; Accepted 26 February 2020; Published 30 March 2020

Academic Editor: Giorgio Besagni

In recent years, the development and construction of islands and reefs has been proposed by the government and commercial company. However, as a large cargo carrier cannot reach islands and reefs if the harbor is not available, such type of carrier which has well deck is designed to meet the requirements of delivering people and equipment. It is a possible way to connect the island and supply cargo ships. This paper firstly summarizes the domestic and foreign research progress of hydrodynamic analysis of ships with well deck. Then, based on the CFD (Computational Fluid Dynamics) tools, we set up a linear numerical wave tank and study the hydrodynamic performance of original Wigley-III ship and modified Wigley-III ship with well deck. The hydrodynamic effect of the floating body in the well deck has been investigated and discussed.

1. Introduction

Recently, with the development of computer technology, various numerical modeling tools are becoming possibility. Compared with the physical model test, the study period of the numerical method is short, the cost is small, and the resource occupancy is low. Moreover, the traditional design mode has been changed by the numerical method and its process is becoming simple.

Longuet-higgins and Cokelet [1] used the Euler–Lagrange method to simulate plunging breaker based on the idea of direct solution of boundary integral. Baker et al. [2] added the artificial damping viscous term to the boundary of a specific free surface in the same way as the sponge absorbed wave energy and presented the concept of damped wave elimination region in the two-dimensional boundary element mode for the first time. Vinje and Brevig [3] proposed the modal decomposition method, which makes the numerical wave tank be capable of dealing with hydrodynamic calculation and motion simulation of floating bodies. Based on completely nonlinear free surface boundary, Jin and Zou [4] established a new vertical two-dimensional wave equation by taking wave surface rise and free surface velocity potential as the variables to be determined. Yan et al. bib5 used the two-point method to separate the wave morphology of each component wave after the submerged body and established a two-dimensional fully nonlinear numerical model to simulate the wave effect on a submerged horizontal cylinder based on the in-domain wave-making technology. Fang et al. [6] used the mixed finite difference and finite volume numerical schemes to solve the two-dimensional fully nonlinear distributed water wave equation and established the fully nonlinear Boussinesq wave propagation numerical model based on the MUSTA scheme. Zhang et al. [7] established a two-dimensional viscous numerical water trough based on the CIP method, which can be used to simulate linear, weakly nonlinear, and strongly nonlinear waves. Li and Ning [8] simulated and studied the deformation of long wave train propagation and the energy exchange between waves of various orders.

Bai and Taylor [9–11] analyzed the phenomenon of fully nonlinear regular wave and focusing wave, respectively, on

vertical cylindrical diffraction and the effect of completely nonlinear wave on fixed and floating structures. Li et al. [12] used high-order spectral methods to simulate three-dimensional fifth-order deep-water Stokes waves to verify accuracy and convergence. Chen et al. [13], based on the CIP method for the gas-liquid two-phase flow numerical model, carried out numerical simulation of the propagation and deformation of solitary waves on coastal slopes. Wu et al. [14] studied the effects of wavelength, water level, effective wave height, and friction resistance on the propagation deformation of near-shore waves.

Many effective methods have been derived for the numerical simulation of the interaction between waves and structures. Presently, the hydrodynamic analysis of ships with well deck is based on the viscous flow theory, which can realize the numerical simulation of the coupled response of ship motion and flow field generated in well deck.

Hopman et al. [15] realized the test of two ship models (with good performance and newly designed) through a typical model test program, made the model in different modal time periods, and simulated the ship model test in a series of wave directions and speeds under two irregular spectral conditions. Subsequently, Bass et al. [16] used the commercial CFD integration code with ship motion code (MOTSIM, a 3D nonlinear time domain program) to simulate the wave interaction in the wetted well deck and verified the numerical simulation results with the model test. Cartwright et al. [17] used SPH (Smoothed Particle Hydrodynamics) method to simulate 2D landing craft containing well deck and explore the influence of well-deck design on landing craft movement. Yoon and Seo [18] conducted model tests on landing craft with different well-deck positions and studied their seakeeping and safety, respectively.

In this work, a simplified ship model is used to verify the effectiveness of the numerical tank. Based on the published Wigley-III ship model data, the numerical simulation of ship diffraction in waves is conducted based on the CFD method. Firstly, the heave and pitch motions of the ship and the modified ship are simulated and compared with the test data of DUT (Delft University of Technology) [19, 20]. Secondly, the heave and pitch motion of the Wigley-III ship model are simulated. Finally, an attempt is made to simulate the motion of well deck with floating structures, so as to provide an effective technical scheme for relevant study.

2. Numerical Method

2.1. Governing Equation and Calculation Algorithm. Continuous equation and Navier–Stokes equation were applied as the governing equation of an incompressible flow as follows:

$$\frac{\partial U_i}{\partial x_i} = 0,$$
$$\frac{\partial U_i}{\partial t} + U_i \frac{\partial U_i}{\partial x_i} = -\frac{1}{\rho}\frac{\partial p}{\partial x_i} + \frac{\partial}{\partial x_i}\left(\nu \frac{\partial U_i}{\partial x_i} - \overline{u_i u_i}\right) + g_i, \quad (1)$$

where U is the velocity, which has three components in x, y, and z direction, respectively, ρ is the density, t is the time, x is the coordinate, p is the pressure, ν is the kinetic viscosity, $-\overline{u_i u_i}$ is the turbulent stress, and g is the acceleration due to gravity. ICEM CFD and ANSYS FLUENT are used for grid generation and for the numerical simulation, respectively. FLUENT is based on the Finite Volume Method (FVM), in which governing equation has been discretized by the FVM.

The Computational Fluid Dynamics (CFD) package, FLUENT, has been successfully utilized to solve the fluid and fluid-structure interactions, and it is used as a basic solver with User Defined Functions (UDF) in this work. To ensure accurate results, we adopt the following settings. (1) The pressure staggering option (PRESTO) discretization scheme is used to solve the pressure. (2) The quadratic upwind interpolation of convective kinematics (QUICK) algorithm is used to discretize the momentum. (3) The pressure implicit with splitting of operators (PISO) algorithm is used for the pressure velocity coupling. (4) The volume of fluid (VOF) method is adopted to capture the water surface. (5) The RNG k-ε model (2eqn) is used to simulate the flow of the incompressible and viscous fluid.

To deal with the wave and structure interaction in the Numerical Wave Tank (NWT), the work adopts the C programming language into the basic solver through UDF. The UDF is used to deal with the wave-generating boundary conditions in the inlet boundary, the wave absorbing zone in the end of the Numerical Wave Tank.

2.2. Boundary Conditions. Generally, the top boundary of the computation domain is taken as a pressure inlet, the bottom boundary of the computation domain is the wall, which depends on the depth, and the left- and right-side boundaries of the computation domain are set as symmetry. The setting of the left inlet wave boundary of the wave-generating area and the right-end boundary of the wave-eliminating area needs to be adjusted according to the calculation, as presented in Figure 1. The other boundaries are also adjusted accordingly to the calculation which can be performed stably.

3. Numerical Wave Tank and Its Validation

3.1. Numerical Model and Mesh Discretization for NWT. The calculation domain is designed as a length of 25 m, a width of 2 m, and a depth of 3 m. The distance between calm water surface and pressure inlet boundary is 1 m and the water depth is 2 m. The end of tank is the wave elimination area, which is 10 m, as shown in Figure 1.

In Figure 1, G1, G2, G3, and G4 are the wave elevation probe, which is located at $x = 2.5$ m, $x = 5$ m, $x = 10$ m, and $x = 25$ m to monitor the corresponding wave height, respectively.

The model is meshed by ICEM CFD module of ANSYS. In the longitudinal direction of the main computational domain, the meshes are distributed equally along the wave

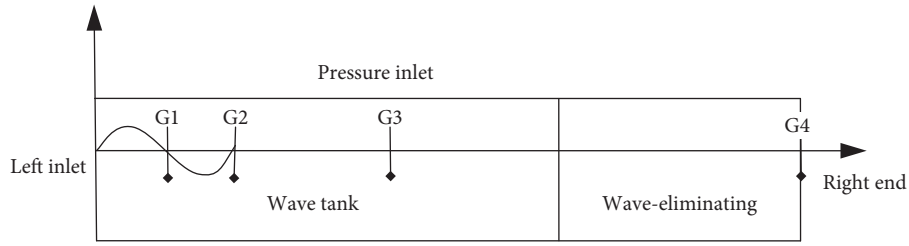

Figure 1: The numerical wave tank and boundaries.

propagation direction; however, in the wave-eliminating region, the meshes gradually become bigger, which can reduce the total number of grids, the operation time, and can improve the calculating efficiency, meanwhile which can result in numerical dissipation. In the vertical direction, according to the water wave theory, the grid is encrypted near the water surface, in order to capture the accurate position of the free surface and improve the numerical accuracy. The place, which is far away from the free surface, will become sparse gradually. In the transverse direction, the grid is divided equally, as shown in Figure 2.

3.2. Convergent Study for NWT. In the numerical solution, mesh discretization and time interval are the most important factors which affects the simulation accuracy, and the numerical solutions have to be stable with the improvement of mesh encryption skill and time interval. Thus, the convergence analysis of the numerical wave tank is carried out and the wave parameter for the simulation is described in Table 1.

The convergence study of time interval has been carried out firstly and has been presented in Figure 3. It can be obtained that convergent results of wave height with different incident wavelength can be found while time interval is less than 0.01 s.

We also consider the study of the mesh density, which is represented by the number of cells Nx in the longitudinal direction within each wavelength and Nz in vertical direction per wave height. We can find that good and convergent results can be obtained when Nx is great than 50 and Nz is great than 25, as shown in Figures 4 and 5. $Nx = 50$ and $Nz = 30$ will be applied for the following simulations, and the snapshot of free surface can be found in Figure 6.

We can also find the time history results of wave elevation at different probes ($x = 2.5$, $x = 5$, and $x = 10$) and good agreements can be obtained by comparing the present CFD results and theoretical value, as shown in Figures 7–9, respectively. We can conclude that the present tank can be used for long time simulations. From comparison, we can also find the nonlinear phenomenon because of the nonlinear governing equation. It has typical nonlinear effect that the peaks and troughs of waves show asymmetric.

The efficiency of wave elimination can be found in Figures 10 and 11. High efficiency wave-eliminating result can be obtained in the present model as the wave-eliminating technology has been involved in the end of the tank.

4. Wave Diffraction of Wigley-III Ship Model

4.1. Numerical Model for Wave Diffraction of Wigley-III Ship Model

4.1.1. Calculation Model of Wigley-III. The model for this calculation is Wigley-III ship model [19, 20]. Journée evaluated the motion of the four kinds of Wigley through the experimental analysis. This paper will use the Wigley-III model, and the main dimensions are shown in Table 2.

In Cartesian coordinate system $o\xi\eta\zeta$, the origin of coordinates o is located on the steady water in the middle of the Wigley-III ship and it can be described mathematically by equation (2). Figures 12 and 13 display the exact shape of the ship in 2D and 3D, respectively:

$$\eta = \left(1-\zeta^2\right)\left(1-\xi^2\right)\left(1+a_2\xi^2+a_4\zeta^2\right)+\alpha\zeta^2\left(1-\zeta^8\right)\left(1-\zeta^2\right)^4,$$
$$a_2 = 0.2,\ a_4 = 0,\ \alpha = 0, \quad (-0.5 \le \xi \le 0.5,\ -0.5 \le \eta \le 0.5,\ 0 \le \zeta \le 1). \tag{2}$$

4.1.2. Boundary Conditions. The inlet boundary is a velocity inlet, which is defined by UDF. When the wave passes through the wave elimination area, the right end should be stationary; thus, the right end boundary can be set as pressure-outlet. The top of the tank is set as pressure-outlet boundary condition. The bottom and the surface of Wigley-III are set as wall boundary conditions. Both sides of the numerical wave tank are set as symmetrical boundary conditions.

4.2. Numerical Simulation and Discussion of Wave Diffraction Case. The test data can be used to verify the simulation results in the numerical wave tank. Journée [20] provided the data of the Wigely model in regular wave, which will be adopted for the comparison in this work.

4.2.1. Numerical Model Setting. In this paper, numerical simulation is carried out by using the Wigley-III ship model under the incident wave and with forward speed. The calculation parameters are shown in Table 3.

4.2.2. Numerical Results with Incident Wave Direction $\beta = 180^\circ$. Figures 14 and 15 show the comparison of the hydrodynamic force amplitude in longitudinal direction

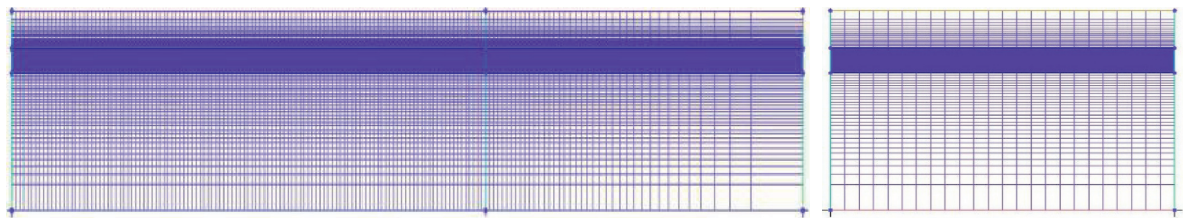

Figure 2: The side view of tank and mesh discretization.

Table 1: The wave parameter for convergent study (wavelength $\lambda = 5$ m).

Wave length (m)	Amplitude (m)	Velocity (m/s)	Period (s)
5.0	0.125	2.776	1.8

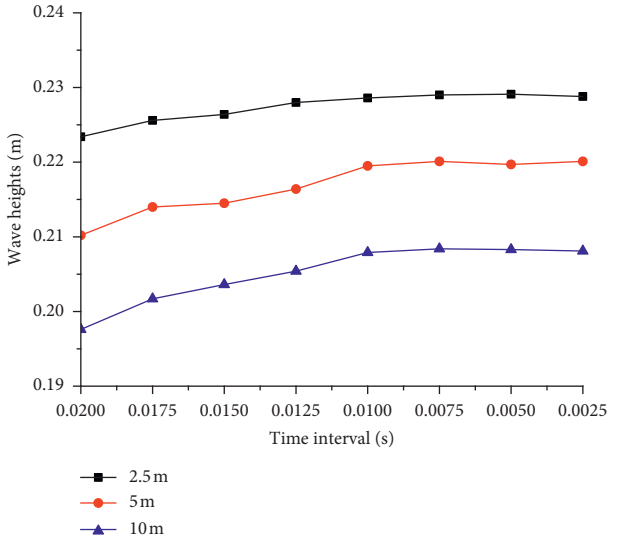

Figure 3: The variation of wave height with different wavelengths and time intervals.

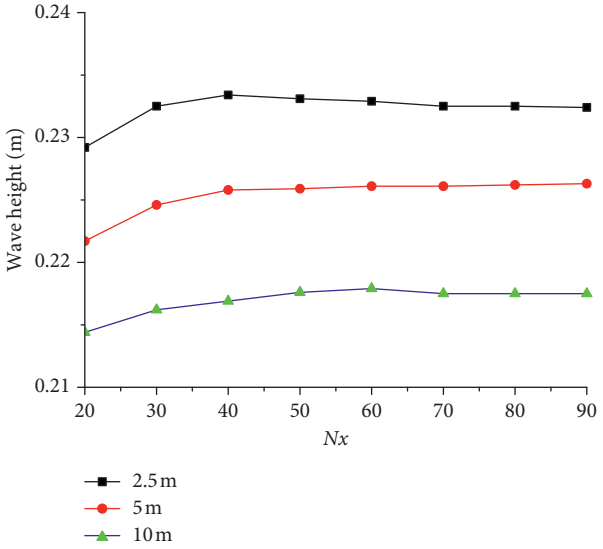

Figure 4: The variation of wave height with different wavelengths and Nx.

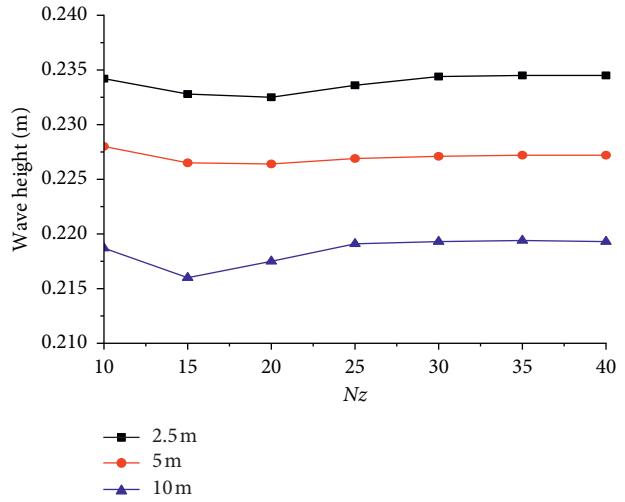

Figure 5: The variation of wave height with different wavelengths and Nz.

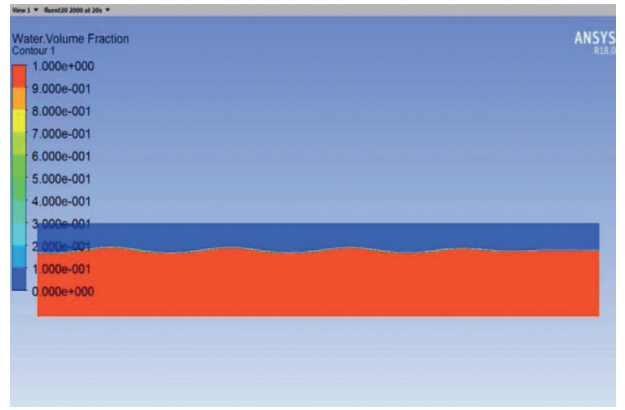

Figure 6: The snapshot of free surface at time $t = 35$ s.

(X_{w1a}) and the coefficient of the corresponding force (X''_{w1a}). X_{w1a} and X''_{w1a} can be calculated by the following equation:

$$\begin{cases} X''_{w1a} = \dfrac{X_{w1a}}{(kA \cdot \rho g \nabla)}, \\ X''_{w3a} = \dfrac{X_{w3a}}{(A \cdot C_{33})}, \\ X''_{w5a} = \dfrac{X_{w5a}}{(kA \cdot C_{55})}. \end{cases} \tag{3}$$

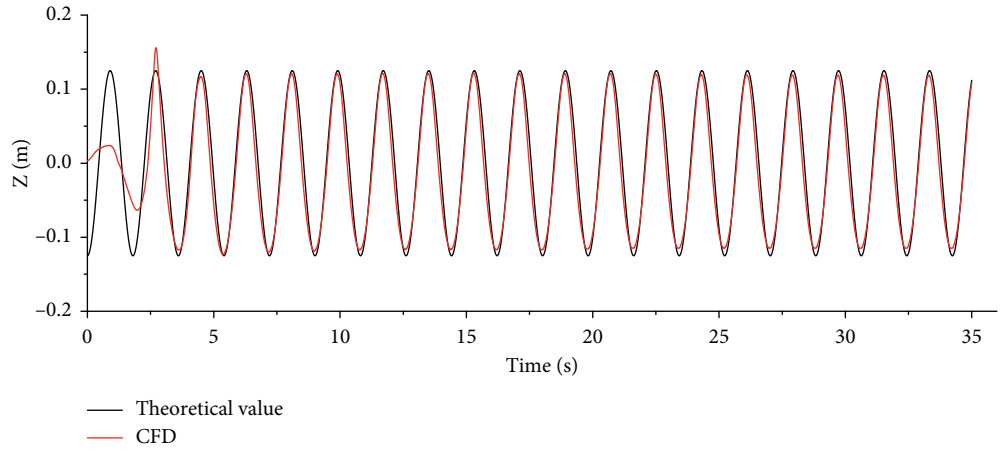

Figure 7: Time history of wave elevation at probe G1 ($x = 2.5$ m).

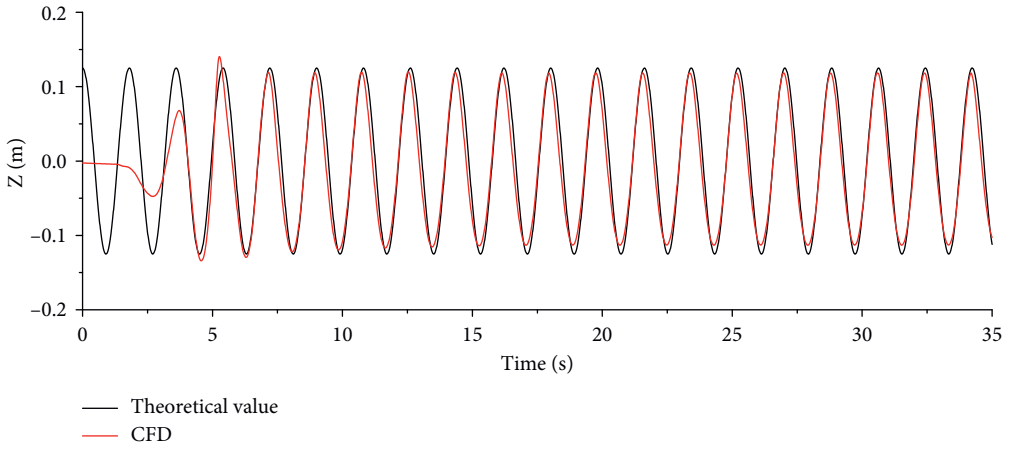

Figure 8: Time history of wave elevation at probe G2 ($x = 5$ m).

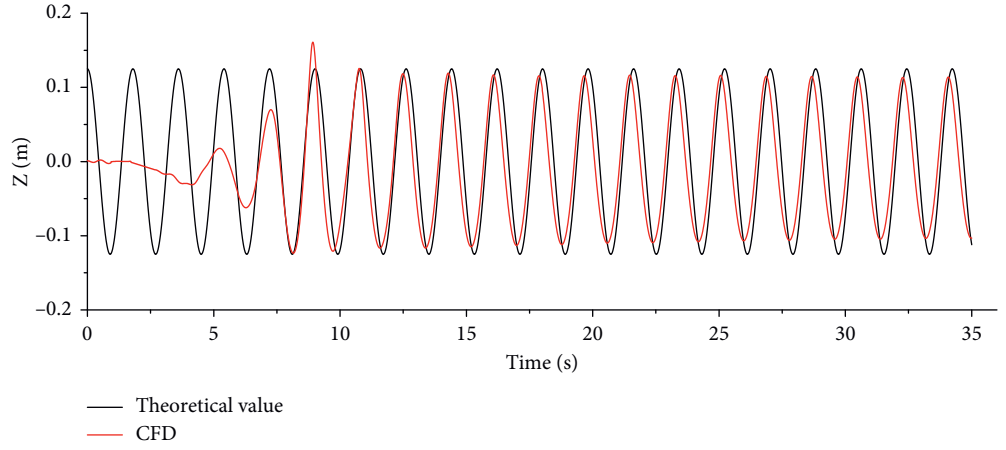

Figure 9: Time history of wave elevation at probe G3 ($x = 10$ m).

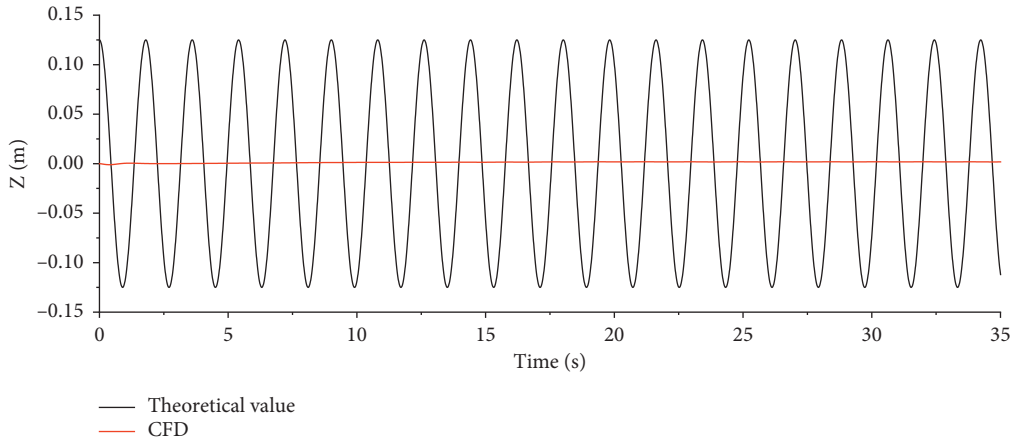

Figure 10: Time history of wave elevation at probe G4 ($x = 25$ m, right-end boundary).

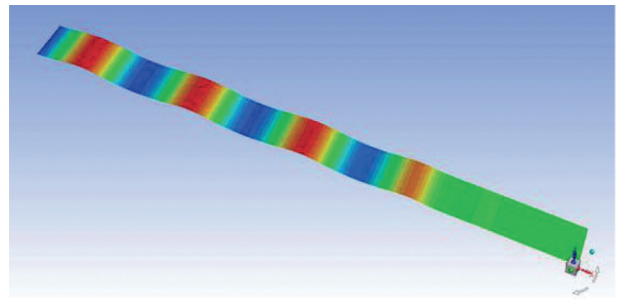

Figure 11: The profile of the free surface.

Table 2: The main dimensions of the Wigley-III ship model.

Parameter and its unit	The value
C_m	0.6667
$L(m)$	3.0000
$B(m)$	0.3000
$d(m)$	0.875
$\nabla(m^3)$	0.0780

By comparing the experimental data, it can be found that the CFD simulation results in this work are in good agreement with the experimental data. Figures 16 and 17 show the heave force X_{w3a} and its coefficient X''_{w3a} and their comparison with the test data.

The numerical results are in good agreement with the experimental results and the heave force of the ship model in the case of heading wave increases with the wavelength, and the relative error is very small.

Figures 18 and 19 show the pitch force and its coefficient under the incident heading wave condition. It can be seen that the calculated results in this work are in good agreement with the experimental data.

4.2.3. Numerical Results at Incident Wave Direction $\beta = 150^\circ$. From the numerical results of wave force in the previous section, the CFD results in this paper agree well with the test data. The method adopted in this paper can simulate the ship sailing in heading waves. However, the sea state is random including wave direction and wave period, and we need to consider the typical wave angle such as $\beta = 150^\circ$ and 3D BEM [21] results will be used for comparison.

Figure 20 shows the coefficient of exciting force on the Wigley-III ship model under six degrees of freedom. As we can see that the dimensionless coefficient of force in waves are in good agreement with the results of the potential flow theory. For the long wave simulation, the CFD results in this paper are slightly larger than that of potential flow theory. The reason [22, 23] is that it has a serious inaccuracy in the flow field near the wave surface when the potential flow is used to solve the velocity problem. It has been solved by Duan et al. and the technology has been used in China Numerical Tank.

5. Hydrodynamic Study of Wigley-III with Floating Body in the Well Deck

5.1. Numerical Model for Case with Floating Body in the Well Deck

5.1.1. Modified Wigley-III Ship Model. The public data for the ship with well deck cannot be found in the database, so we set a ship with well deck artificially. In order to analyze

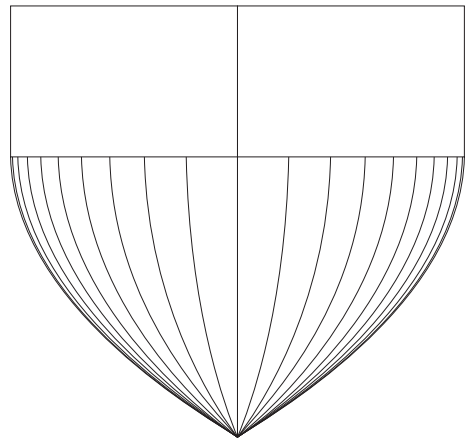

Figure 12: The shape of Wigley-III.

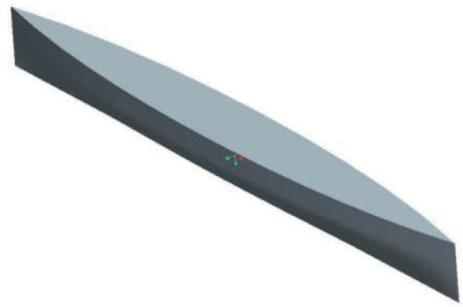

Figure 13: The 3D model of Wigley-III.

Table 3: The parameters for wave diffraction case.

Item	Parameter and its unit	Value
F_r		0.2, 0.3
Amplitude of the incident wave	A (m)	0.023–0.025
The incident wavelength	λ(m)	1.5, 2.25, 3.0, 3.75, 4.5, 5.25, 6.0
Wavelength/length of ship	λ/L	0.5, 0.75, 1.0, 1.25, 1.5, 1.75, 2.0
Incident wave direction	(°)	150, 180

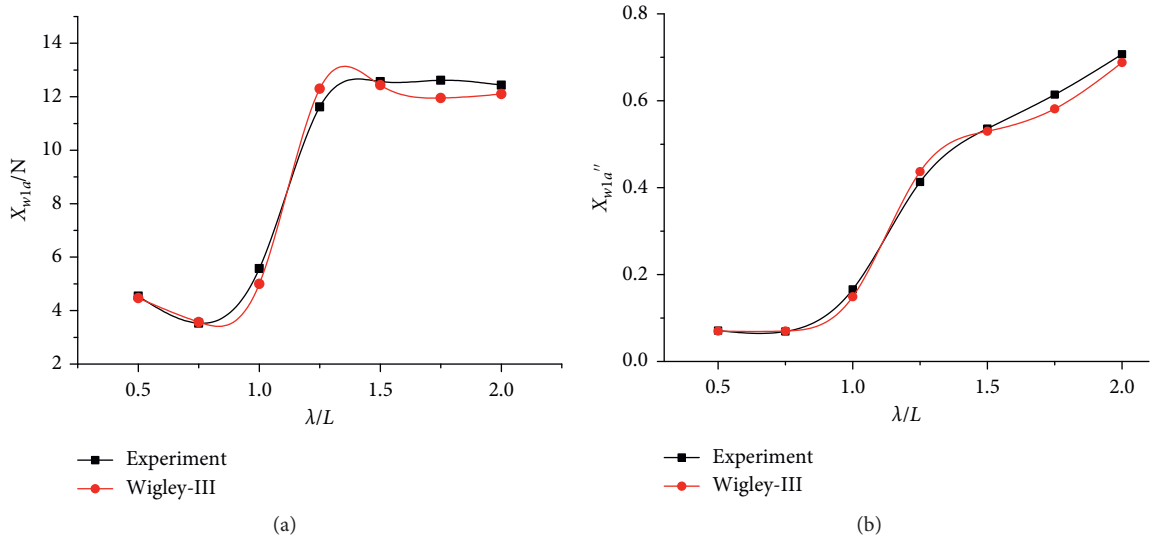

Figure 14: Surge and its coefficient at F_r = 0.2 in heading waves (β = 180°). (a) Surge. (b) Coefficient.

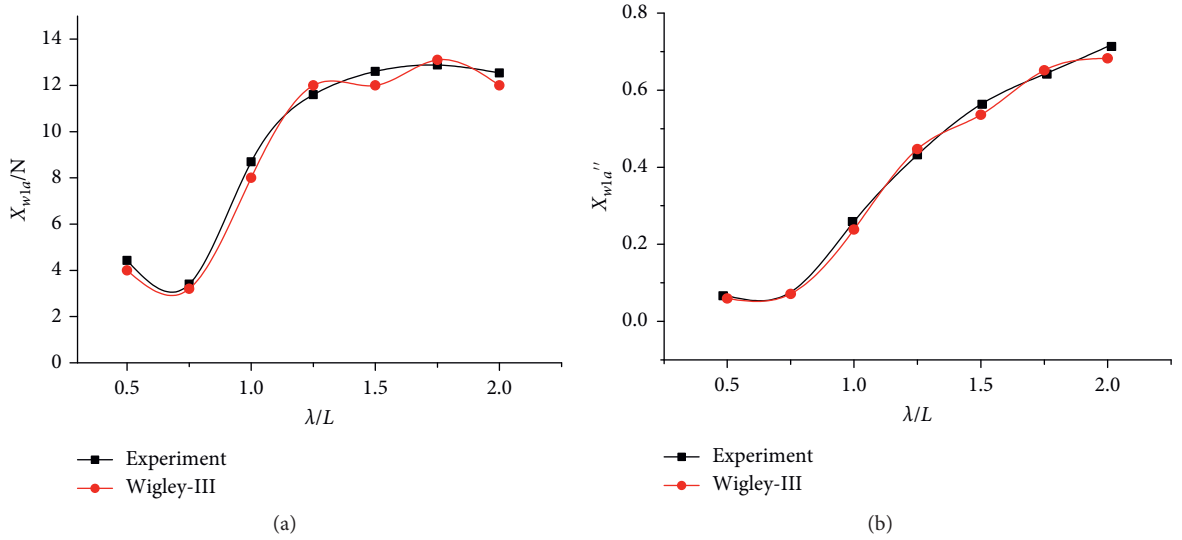

Figure 15: Surge and its coefficient at $F_r = 0.3$ in heading waves ($\beta = 180^\circ$). (a) Surge. (b) Coefficient.

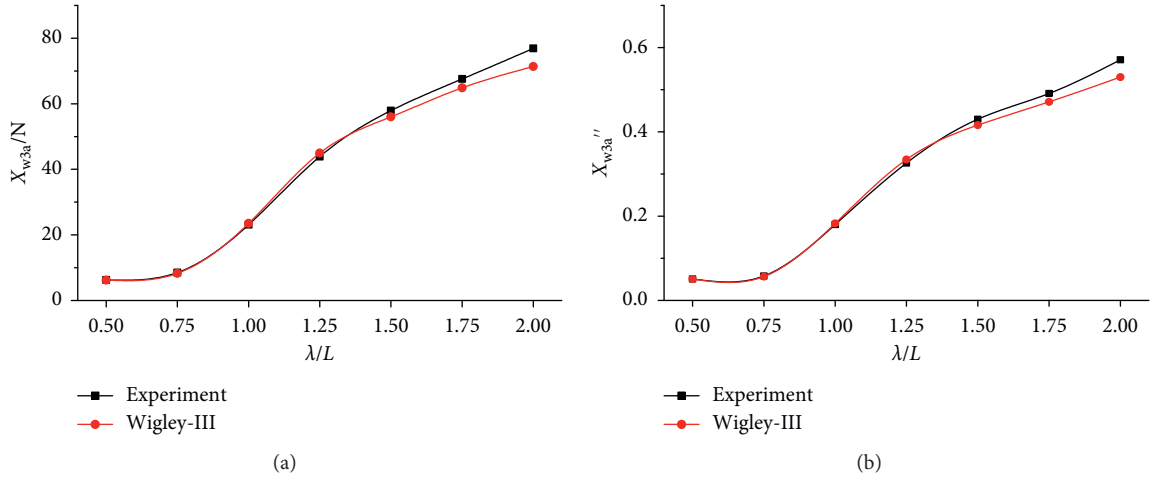

Figure 16: Heave and its coefficient at $F_r = 0.2$ in heading waves ($\beta = 180^\circ$). (a) Heave. (b) Coefficient.

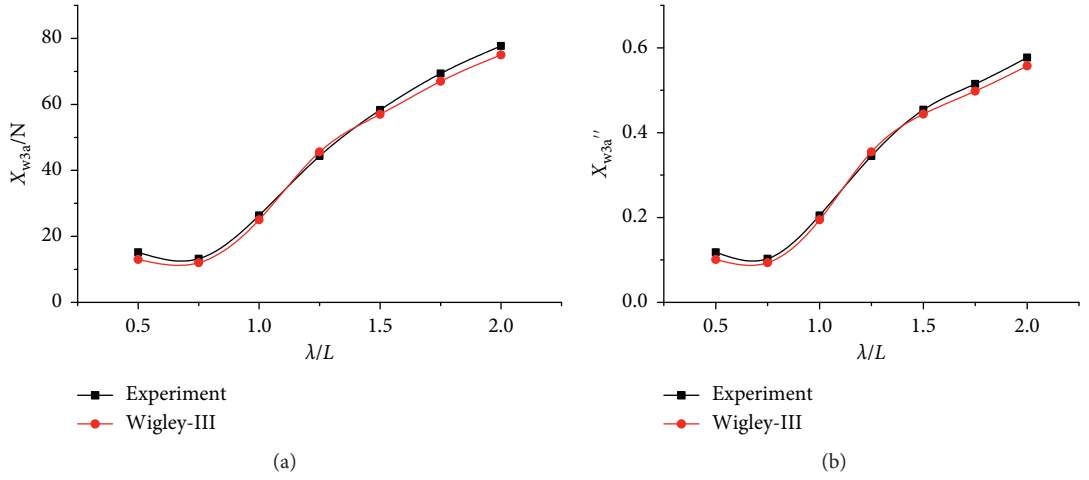

Figure 17: Heave and its coefficient at $F_r = 0.3$ in heading waves ($\beta = 180^\circ$). (a) Heave. (b) Coefficient.

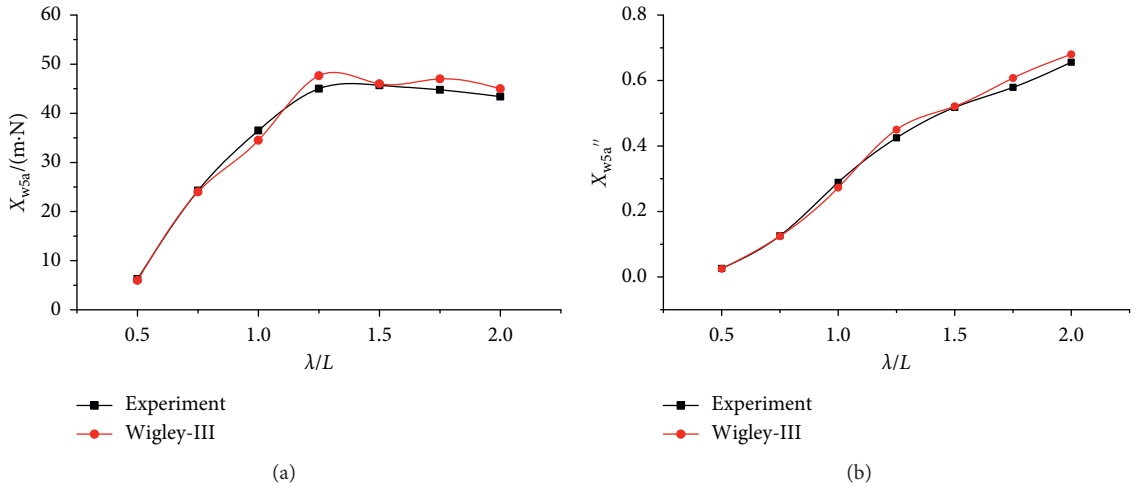

Figure 18: Pitch and its coefficient at $F_r = 0.2$ in heading waves ($\beta = 180^\circ$). (a) Pitch. (b) Coefficient.

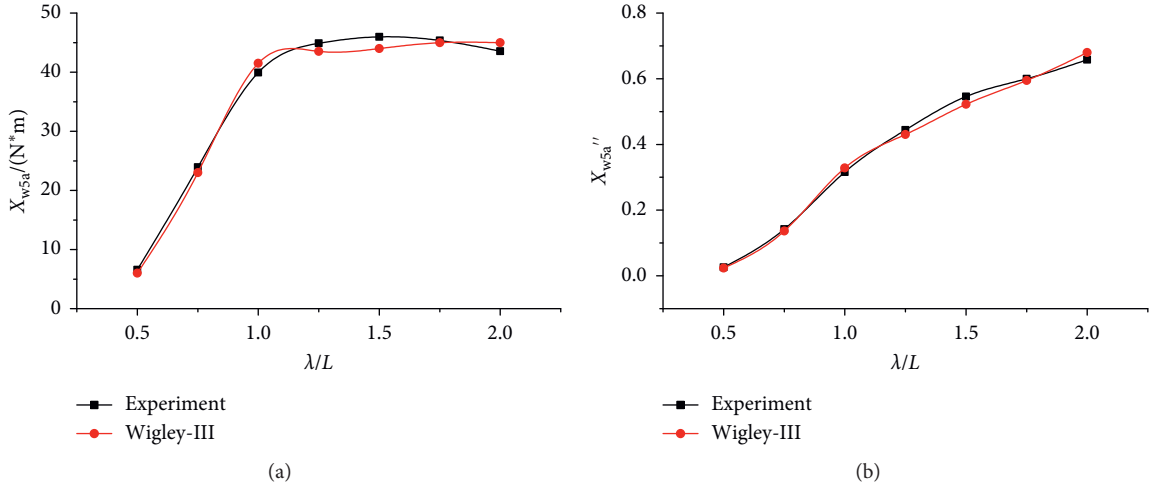

Figure 19: Pitch and its coefficient at $F_r = 0.3$ in heading waves ($\beta = 180^\circ$). (a) Pitch. (b) Coefficient.

the effect of floating body, the model is based on the original Wigley-III ship model. A well deck of 0.15 m width and 0.2 m height was built at the stern of the ship, named the modified Wigley-III ship model. Details can be found in Figure 21. Note that the shape of the present ship model is quite different from that of the actual ship with well deck, and further study should be executed by a more appropriate ship model.

5.1.2. The Model with Small Floating Body in the Well Deck. Based on the modified Wigley-III ship, a small floating structure has been put into the well deck to analyze its effect and multibody interaction. The floating body in the well deck is simplified with a rectangular floating object for the convenient calculation. The model is shown in Figure 22 and the parameters can be found in Table 4.

5.2. Numerical Results and Discussion

5.2.1. Numerical Model Setting. When the well deck is opened and the floating body exits in the well deck, the hull is mostly at zero forward speed; thus, this part focuses on the motion of the hull without forward speed. In the numerical wave tank, the Wigley-III ship model, the modified Wigley-III ship model, and the modified Wigley-III ship model containing the floating body in the well deck has been calculated and compared. The parameters for the simulation are given in Table 5.

5.2.2. Numerical Results with Heading Waves $\beta = 180^\circ$. The hull, encountering different incident heading waves, has been calculated. The obtained results are shown in Figures 23 and 24. It can be seen that the numerical results are consistent with the experimental data.

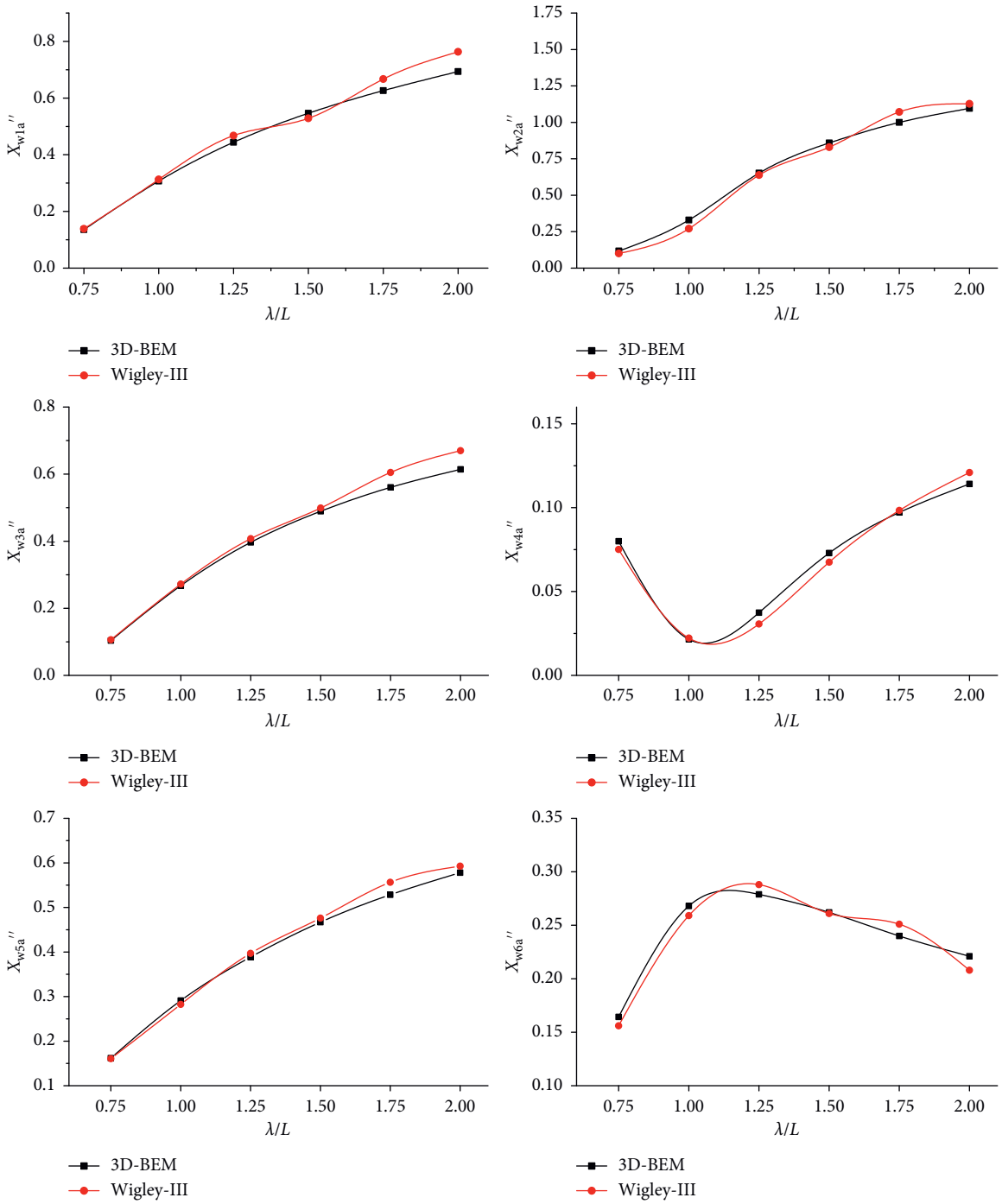

Figure 20: The coefficient of exciting force on the Wigley-III ship model in waves with $\beta = 150^{\circ}$.

In Figure 23, the results of the modified Wigley-III ship model has a similar trend with the original Wigley-III ship model, and it can be clearly seen that the heave coefficient of the modified Wigley-III ship model is reduced when the wavelength is greater than the length of the ship. It means that the well deck is good for the heave motion.

For the pitch, as shown in Figure 24, the trend of the ship model with the well deck changes significantly with the short waves. The amplitude of pitch motion increases significantly when $\lambda/L = 0.5$. We can also find that the well deck has disadvantage for the pitch motion. Through comparing the motions, it is found that the floating body in the well deck has small effect on the overall motion of the ship.

5.2.3. Numerical Results at Incident Wave Direction $\beta = 45^{\circ}$. Figures 25 and 26 show the heave and pitch of the ships at incident wave direction $\beta = 45^{\circ}$. The coefficient of them has been presented in Figures 27 and 28. It can be seen that the motions of ships tend to be consistent and have same trend.

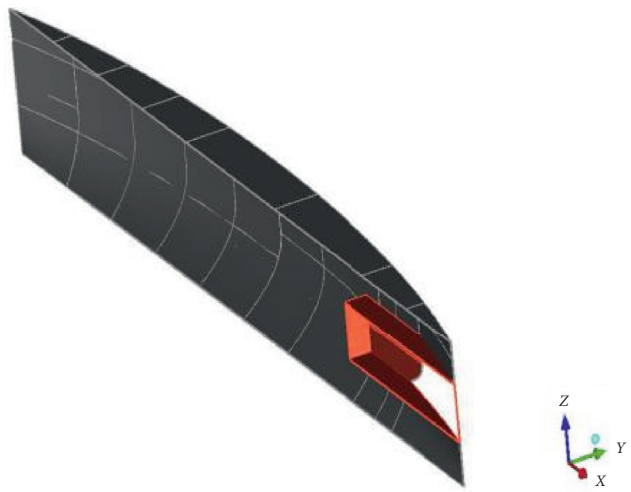

Figure 21: The model of the modified Wigley-III with well deck at stern.

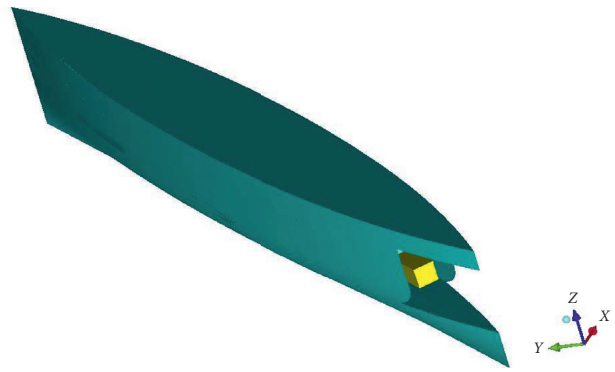

Figure 22: Modified Wigley-III ship model with the floating body in the well deck.

Table 4: Main parameters of modified Wigley-III.

Item	Parameter and its unit	Value
Distance from motion center to baseline	$\overline{KR}$ (m)	0.1875
Distance from center to baseline	$\overline{KG}$ (m)	0.1700
Radius of inertia for pitch	k_{yy} (m)	0.7500

Table 5: The parameters for numerical simulation.

Item	Parameter and its unit	Value
The incident wave amplitude	A(m)	0.013–0.022
The incident wavelength	λ(m)	1.5, 2.25, 3.0, 3.75, 4.5, 5.25, 6.0
Wavelength/length of ship	λ/L	0.5, 0.75, 1.0, 1.25, 1.5, 1.75, 2.0
Wave direction	(°)	45, 180

Figure 27 shows that the heave motion of the ships increases with the wavelength, and the amplitude of the heave motion increases, and becomes closer to a stable value. Compared to the original Wigley-III ship, the pitch motion of the modified Wigley-III ship model becomes more obvious when the wavelength is greater than the length of the ship and the amplitude of pitch motion is reduced, as shown in Figure 28. We may conclude that the floating body does not

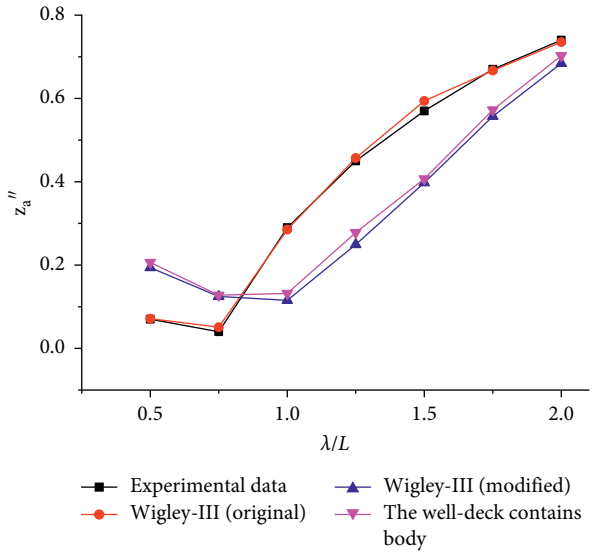

Figure 23: Coefficient of heave for different Wigley-III ship models.

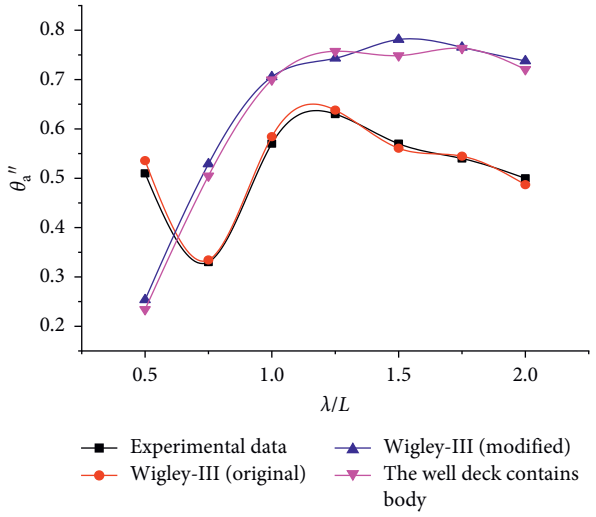

Figure 24: Coefficient of pitch for different Wigley-III ship models.

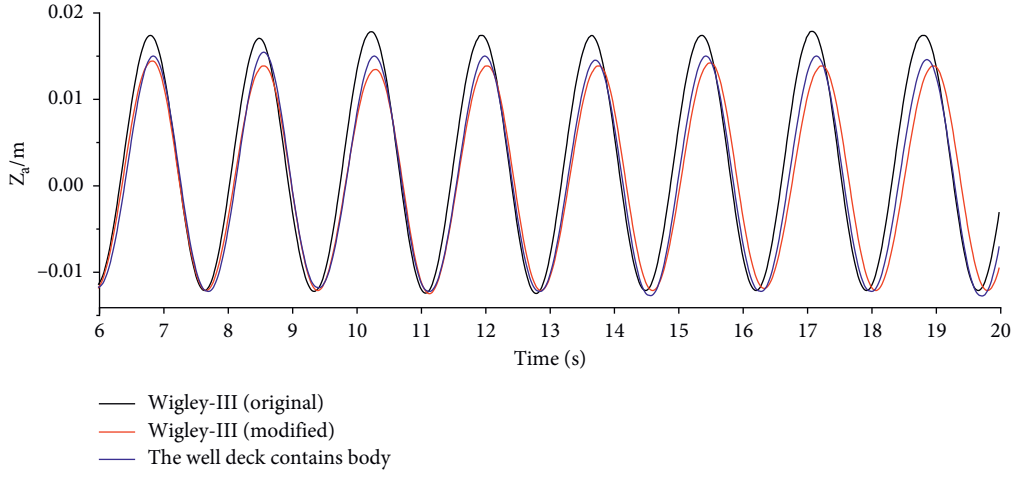

Figure 25: Time history of heave motion of ships at $\beta = 45^{\circ}$.

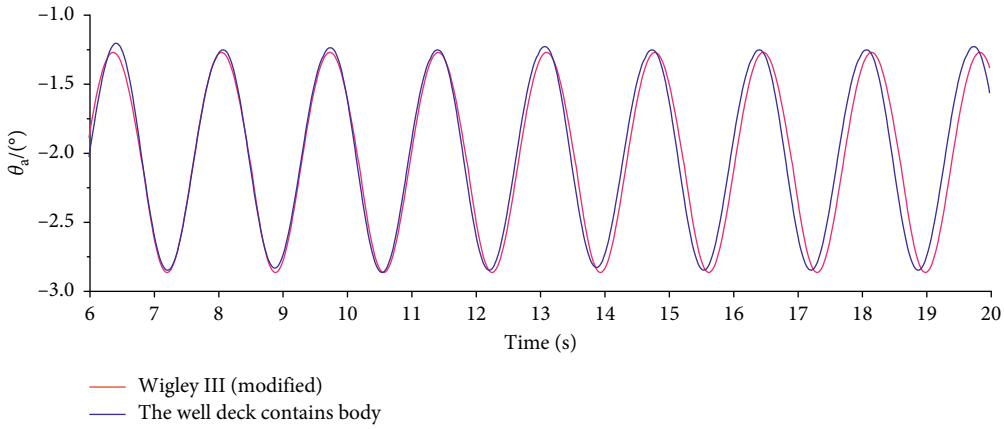

Figure 26: Time history of pitch motion of ships at $\beta = 45^{\circ}$.

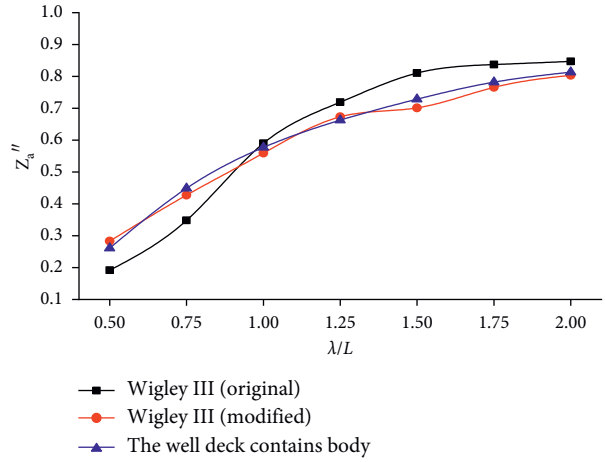

Figure 27: Coefficient of heave for ships at $\beta = 45^{\circ}$.

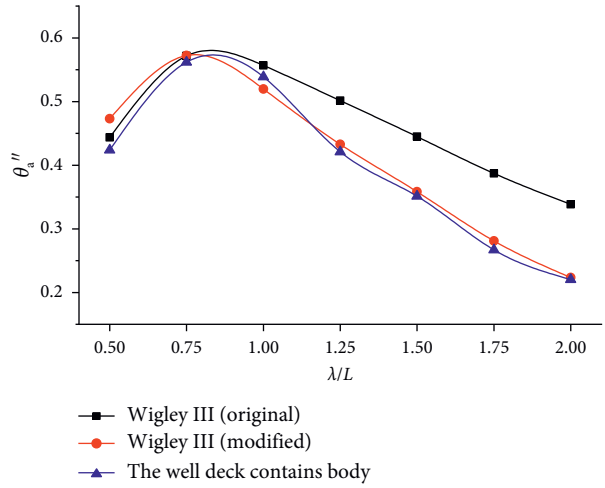

Figure 28: Coefficient of pitch for ships at $\beta = 45^{\circ}$.

have serious effect on the modified Wigley-III ship. Later, we may focus on the motion of the floating body in the well deck in the high sea state.

6. Conclusion

Based on CFD (Computational Fluid Dynamics) tools, this paper uses FLUENT to simulate the Wigley-III ship model in three-dimensional linear numerical wave tank and the modified Wigley-III ship with well deck also has been investigated. Through the calculation we have conclusions as below:

(1) Based on the Navier–Stoke governing equation, the VOF method was used to capture the water surface, and the RNG turbulence model was used to solve the numerical wave tank. The effects of mesh discretization and time interval have been presented and discussed. We found that the time interval has much greater effect on the accuracy of numerical simulation when the mesh discretization is fixed. We can obtain accurate results when regular wave propagates in the numerical wave tank by using the present model.

(2) As the public data for ships with well deck is not available, we modified the stern of the original Wigley-III ship model. The numerical simulation for the original Wigley-III ship and modified Wigley-III ship with the well deck has been carried out, and the numerical results are in good agreement with the experimental data for wave diffraction problem and the motion of the modified model is similar to that of the original ship.

(3) We also found that the floating body did not have significant effect on the modified Wigley-III ship with the well deck. For the further study, we should consider the ship under the high sea state and predict the motion of the floating body in the well deck.

Data Availability

The data used to support the findings of the study are available from the corresponding author upon reasonable request.

Conflicts of Interest

The authors declare that they have no conflicts of interest.

Acknowledgments

This work was supported by the National Natural Science Foundation of China (Grant nos. 51709137 and 51879125), Key University Science Research Project of Jiangsu (Grant no. 18KJA130001), Marine Equipment and Technology Institute of Jiangsu University of Science and Technology Funding Project (Grant no. HZ20190922), and Postgraduate Research and Practice Innovation Program of Jiangsu Province (Grant nos. KYCX18_2343 and SJCX19_1187).

References

[1] M. S. Longuet-Higgins and E. D. Cokelet, "The deformation of steep surface waves on water- i. a numerical method of computation," *Proceedings of the Royal Society A: Mathematical, Physical and Engineering Sciences*, vol. 350, no. 1660, pp. 1–26, 1976.

[2] G. R. Baker, D. I. Meiron, and S. A. Orszag, "Application of a generalized vortex method to nonlinear free surface flows," in *The proceedings, Third International Conference on Numerical Ship Hydrodynamics*, pp. 179–191, Paris, France, June 1981.

[3] T. Vinje and P. Brevig, "Nonlinear ship motions," in *Proceedings of the International Conference on Numerical Ship Hydrodynamics*, Paris, France, June 1981.

[4] H. Jin and Z. Zou, "Hyperbolic mild slope equations with inclusion of amplitude dispersion effect: regular waves," *China Ocean Engineering*, vol. 22, no. 3, pp. 431–444, 2008.

[5] B. Yan, H. Lin, and D. Ning, "Nonlinear numerical simulation of the effect of waves on submerged horizontal cylinders," *Marine Sciences Progressive*, vol. 31, no. 3, pp. 319–325, 2013.

[6] K. Z. Fang, L. Wang, Z. B. Liu, and Z. L. Zou, "A fully nonlinear boussinesq model for wave propagation based on MUSTA scheme," *Chinese Journal of Theoretical & Applied Mechanics*, vol. 46, no. 5, pp. 647–654, 2014.

[7] D. H. Zhang, J. D. Wang, and G. H. He, "Numerical simulation of strongly nonlinear waves," *Proceeding of National Symposium on Hydrodynamics*, vol. 1, in Chinese, 2015.

[8] X Li and D. Ning, "Simulation study on propagation characteristics of long wave train," *Hydrodynamics Research and Progress (Series A)*, vol. 33, no. 6, pp. 714–719, 2018.

[9] W. Bai and R. E. Taylor, "Higher-order boundary element simulation of fully nonlinear wave radiation by oscillating vertical cylinders," *Applied Ocean Research*, vol. 28, no. 4, pp. 247–265, 2006.

[10] W. Bai and R. E. Taylor, "Numerical simulation of fully nonlinear regular and focused wave diffraction around a vertical cylinder using domain decomposition," *Applied Ocean Research*, vol. 29, no. 1-2, pp. 55–71, 2007.

[11] W. Bai and R. E. Taylor, "Fully nonlinear simulation of wave interaction with fixed and floating flared structures," *Ocean Engineering*, vol. 36, no. 3-4, pp. 223–236, 2009.

[12] J. X. Li, S. X. Liu, and K. Y. Hong, "Numerical simulation of nonlinear waves," *Journal of Dalian University of Technology*, vol. 48, no. 3, pp. 430–435, 2008.

[13] Y. Chen, Z. H. Fang, and X. Z. Zhao, "Numerical simulation of offshore wave evolution," in *Proceedings of the 17th China Ocean (Coastal) Engineering Symposium*, vol. 1, Nanning, China, 2015, in Chinese.

[14] X. W. Wu, W. B. Liu, and T. C. Liu, "Numerical study of wave propagation and deformation characteristics in offshore waters," *Science Technology and Engineering*, vol. 18, no. 33, pp. 126–131, 2018.

[15] H. Hopman, G. K. Kapsenberg, and E. M. Krikke, "Design and hydromechanic aspects of the amphibious transport vessel for the royal Netherlands navy," *Naval Engineers Journal*, vol. 106, no. 3, pp. 163–174, 1994.

[16] D. Bass, D. Molyneux, and K. McTaggart, *Simulating Wave Action in the Well Deck of Landing Platform Dock Ships Using Computational Fluid dynamics*, Warship, Toledo, OH, USA, 2004.

[17] B. Cartwright, M. Renilson, G. MacFarlane, D. McGuckin, and S. Cannon, "Motions of a landing craft in a flooded well dock—effect of well dock design," in *Proceedings of the*

International Conference on Military Support Ships, London UK, November 2007.

[18] S. H. Yoon and K. H. Seo, "Well dock design and assessment of relative motions during the operation of the landing crafts within well dock," *Journal of the Society of Naval Architects of Korea*, vol. 49, no. 2, 2012.

[19] J. M. J. Journée, "Experiments and calculations on four wigley hullforms," in *Society of Naval Architects and Marine Engineers*, Society of Naval Architects and Marine Engineers Headquarters, Jersey City, NJ, USA, 1992.

[20] J. M. J. Journée, *Experiments and Calculations on 4 Wigley Hull Forms in Head waves*, p. 909, Delft University of Technology, Delft, Netherlands, 1992.

[21] Z. Z. Fang, R. C. Zhu, G. P. Miao, and C. Gong, "Numerical simulation of diffraction problems of moving vessels in numerical wave tank," *Journal of Shanghai Jiaotong University*, vol. 46, no. 8, pp. 1203–1217, 2012.

[22] G. Xu, B. C. Khoo, and A. M. S. Hamouda, "Time-domain simulation of second-order irregular wave diffraction based on hybrid water wave radiation condition," *Applied Mathematical Modelling*, vol. 40, no. 7-8, pp. 4451–4467, 2016.

[23] W. Duan, J. Chen, and B. Zhao, "Second-order taylor expansion boundary element method for the second-order wave diffraction problem," *Engineering Analysis with Boundary Elements*, vol. 58, pp. 140–150, 2015.